JOURNAL OF MATERIALS SCIENCE **39** (2004) 5263–5266

The behaviour of highly over-stoichiometric $LaNi_5$ Mn_2 alloy as negative electrode for Ni/MH batteries

F. CUEVAS*, A. MIARD, A. PERCHERON-GUÉGAN
Laboratoire de Chimie Métallurgique des Terres Rares, ISCSA-CNRS, 2-8 rue Henri Dunant, F-94320 Thiais, France
E-mail: fermin.cuevas@glvt-cnrs.fr

Key electrochemical properties of highly over-stoichiometric $LaNi_5Mn_2$ alloy with $CaCu_5$-type structure have been measured and compared with those of stoichiometric $LaNi_4Mn$ alloy. $LaNi_5Mn_2$ is obtained by mechanical alloying of two-phase $La(Ni,Mn)_5 + (Ni,Mn)$ alloy previously produced by induction melting. The as-milled alloy was thermally annealed at 450°C for one hour to crystallise milling-induced amorphous phase. As derived from DSC and XRD measurements, further annealing at 550°C produces segregation of minor NiMn-phase (21 wt%), which leaves stoichiometric $LaNi_4Mn$ alloy (79 wt%) as a major phase. Electrochemical cycle-life and potential equilibrium measurements for both $LaNi_5Mn_2$ and $LaNi_4Mn$ alloys show that the over-stoichiometric alloy has much lower discharge capacity than the stoichiometric one (135 mAh/g and 260 mAh/g, respectively). Conversely, the over-stoichiometric alloy exhibits much better cycle-life than the stoichiometric one (5% and 25% decay capacity after 55 cycles, respectively). These results demonstrate that stoichiometry is an effective parameter for tuning the discharge capacity and cycle-life of $LaNi_{5+x}$-type electrodes to the performances required by a particular application.

1. Introduction

$LaNi_5$ alloy is an outstanding material for hydrogen storage, since it absorbs reversibly one hydrogen per metal atom [1]. Unfortunately, stoichiometric $LaNi_5$ has a poor cycling stability for Nickel/Metal Hydride (Ni/MH) battery applications, which is currently solved by partial substitution of nickel for Mn, Al and costly Co [2]. Recent investigations show that a high electrochemical cycling stability can also be attained in Co-free over-stoichiometric compounds [3–5].

The knowledge of the influence of over-stoichiometry on the hydrogenation properties of $LaNi_{5+x}$ electrodes is constrained by the fact that, in the La-Ni binary system, over-stoichiometry is limited to $x = 0.4$ at equilibrium conditions [6]. However, this limit can be notably crossed by using non-equilibrium preparation methods [7]. Thus, $LaNi_6$ compound was obtained, for instance, by mechanical alloying [8]. However, this alloy can not operate in open-cell Ni/MH batteries, as its hydride plateau pressure reaches 7 atm at room temperature [9]. Such a low hydride stability is promoted by the reduction of the crystallographic unit-cell volume with over-stoichiometry. Hopefully, this problem may be circumvented by partial replacement of Ni by Mn in the base of the higher atomic radius of the latter ($r_{Ni} = 1.24$ Å, $r_{Mn} = 1.35$ Å). As a matter of fact, Mn substitution in stoichiometric $LaNi_{5-z}Mn_z$ alloys is reported to effectively increase hydride stability without reducing the storage capacity of the parent compound [10].

In this work, we report on the preparation of highly over-stoichiometric $LaNi_5Mn_2$ alloy by mechanical alloying and subsequent thermal annealing. The electrochemical activity of this alloy is compared with that of stoichiometric $LaNi_4Mn$ alloy and the reason of their different behaviour is discussed.

2. Experimental

A biphasic alloy with nominal composition $LaNi_5Mn_2$ was initially obtained from induction melting of the pure elements (99.9% purity) under He atmosphere. The ingot was mechanically crushed down to 100 μm, introduced into a stainless-steel vial under argon atmosphere, and mechanically sealed with a Taurus ring. About 10 g of alloy powder were ball milled for 72 h in a planetary ball milling (Fritsch P7) at a rotating speed of 500 rpm with a ball-to-powder ratio of 10:1. The stainless steal balls were 14 mm in diameter. The milled powder was then cold-pressed into pellets at 4 ton/cm^2 and thermally annealed for 1 h at either 450°C or 550°C under secondary vacuum.

*Author to whom all correspondence should be addressed.

Chemical composition of the alloys was studied by electron probe microanalysis (EPMA) in a Cameca SX-100 instrument. Thermal analysis was conducted for the as-milled sample in a TA-Q100 differential scanning calorimeter (DSC) within the temperature range 50–550°C at a linear heating rate of 10°C/min. DSC measurements were performed using an Al pan as sample holder and with an argon gas flow of 50 ml/min. Alloy crystal structure was studied by powder X-Ray Diffraction (XRD) using KCu_α radiation in a Bragg-Brentano θ-θ Brucker D8 Diffractometer equipped with backscattered rear graphite monochromator. XRD patterns were refined by the Rietveld method using the FULLPROF software [11].

Two alloy electrodes were prepared from 450 and 550°C annealed alloy powder, respectively. 90% in mass of alloy powder was mixed with 5% of highly conductive carbon powder and 5% (dry mass) of PTFE solution as a binder. This paste was rolled to produce a sheet 250 μm in thickness. Two pieces from the sheet were cut in squares of $\sim$1cm^2 surface and cold pressed at 4 ton/cm^2 over both faces of a Ni grid collector. The electrode was put into a one-compartment electrochemical cell, which also comprises a $NiOOH/Ni(OH)_2$ counter electrode, a Hg/HgO reference electrode and 5 M KOH electrolyte solution. Charge/discharge cycles were performed by the galvanostatic method (electrode was charged/discharged at 60 mA/g for 5 h) using a MacPile device from Biologic with a cut-off potential of -0.7 V vs. Hg/HgO. Potential equilibrium measurements were done by successive step-wise discharging of the working electrode. A variation of the open-circuit potential lower than 1 mV for a period of 1 h was adopted as the equilibrium condition.

3. Results and discussion

3.1. Alloy characterisation

XRD patterns for induction-melted, mechanically alloyed and thermally annealed (450 and 550°C) alloys are shown in Fig. 1. Induction-melted alloy can be indexed with two phases: a hexagonal $CaCu_5$-type structure and a tetragonal AuCu-type structure. This basically reflects the characteristics of the binary La-Ni phase diagram [6] at high Ni-contents (Ni at% > 83%), where $LaNi_5$ and Ni phases coexist. After the milling process, diffraction peaks exhibit severe broadening, tetragonal lines disappear and only the hexagonal lines remain. Besides, a very wide diffraction halo between $2\theta = 30°$ and 50° is observed. On annealing at 450°C, the diffraction halo disappears without inducing any other significant change on the XRD pattern. Further annealing at 550°C produces peak narrowing, which is again accompanied with the appearance of the tetragonal lines. As a matter of fact, the system recovers on heating its equilibrium configuration.

DSC measurements during heating of the as-milled sample reveal two main exothermic peaks (Fig. 2). The first one occurs at 339°C, with onset temperature at 262°C, and involves a reaction heat of 48 J/g. It is ascribed to a crystallization process as it matches with the disappearance of the diffraction halo in the XRD pattern. The crystallization temperatures here reported

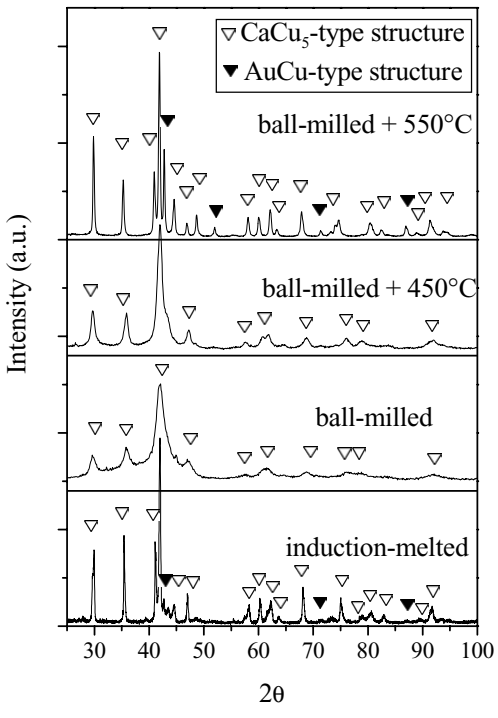

Figure 1 XRD diffraction patterns of the studied alloys. Phase identification is indicated by *X* for the $CaCu_5$-type structure and by *B* for the AuCu-type structure.

concur with previous data on $LaNi_5$-type amorphous alloys [12, 13]. The second DSC peak occurs at 498°C, with onset temperature at 471°C, and involves a much lower reaction heat ($\Delta H = 4.5$ J/g). This peak is ascribed, by comparison with XRD data, to the segregation of the tetragonal phase out of the hexagonal one.

Further insight on the structural alloy properties can be gained by Rietveld analysis of XRD patterns from the annealed samples. Fitting refinements are shown in Fig. 3 and main results are summarized in Table I. For 450°C sample, XRD data can be well fitted to a single-phase $CaCu_5$-type structure having as unit-cell composition $La_{0.77(1)}(Ni,Mn)_{5.46(1)}$. Over-stoichiometry is provided by random partial substitution of La atoms by (Ni,Mn) dumbbells [14, 15]. 22% of La atoms must be substituted by dumbbells to attain this stoichiometry. The reported alloy composition is close to that found by

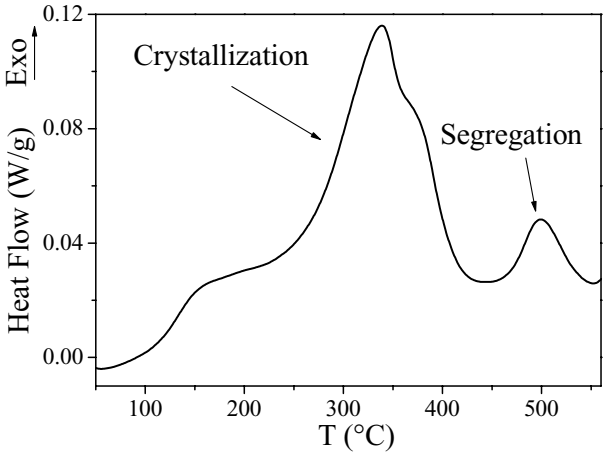

Figure 2 Continuous heating DSC curve of as-milled $LaNi_5Mn_2$ alloy at a heating rate of 10°C/min.

TABLE I Rietveld refinement results of XRD data from 450 and 550°C annealed samples

T (°C)	Phase composition	Structure-type	Content (wt%)	a (Å)	c (Å)	V (Å^3)	D (nm)	R_{wp} (%)	R_B (%)
450	$La_{0.77(1)}(Ni,Mn)_{5.46(1)}$	$CaCu_5$	100	5.0029 (5)	4.1615 (5)	90.20 (2)	8 (1)	6.8	5.3
550	$La_{1.00(1)}$ $(Ni,Mn)_{5.00(1)}$	$CaCu_5$	74 (1)	5.0784 (1)	4.0599 (1)	90.677 (4)	35 (5)	7.8	3.7
	(Ni,Mn)	AuCu	26 (1)	3.7337 (1)	3.5124 (2)	48.964 (3)	25 (5)	7.8	2.5

a, c and V are the unit-cell parameters and volume of the identified phases; D is the average crystallite size; R_{wp} and R_B are the weighted-profile and Bragg agreement factors; e.s.d.s. in parentheses.

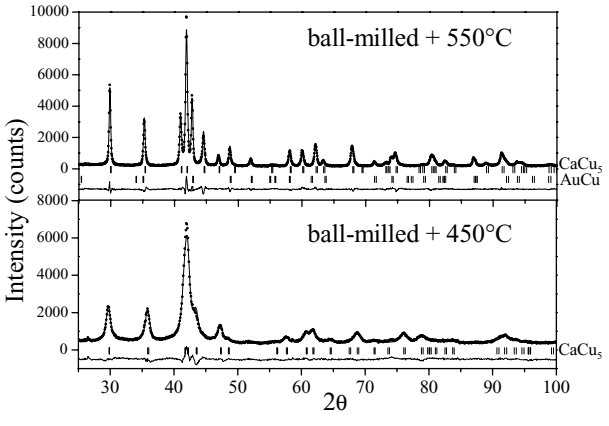

Figure 3 Rietveld refinements of XRD patterns of ball-milled $LaNi_5Mn_2$ alloy after thermal annealing at 450°C (bottom) and 550°C (top). The observed (points), calculated (line) and difference (bottom line) patterns are shown. Vertical bars correspond to peak positions of $CaCu_5$-type and AuCu-type structures.

EPMA analyses $La_{1.00(1)}Ni_{5.00(1)}Mn_{1.94(2)}$. As concerns 550°C sample, its XRD pattern exhibits a two-phase contribution consisting of a stoichiometric $La(Ni,Mn)_5$ majority phase and a (Ni,Mn) minority phase. It is worth remarking that peak intensity in XRD patterns is rather independent on relative concentration of Ni and Mn atoms because these elements possess close electronic charge density. However, owing to their difference in atomic radii ($r_{Ni} = 1.24$ Å, $r_{Mn} = 1.35$ Å), Mn-substitution produces significant lattice volume expansion in stoichiometric $LaNi_{5-z}Mn_z$ ($0 < z < 2$) alloys. Considering the volume cell given in Table I and the reported cell expansion, $V(Å^3) = 86.42 + 4.61\ z$ [10], the major phase composition is evaluated as $LaNi_{4.08}Mn_{0.92}$. This composition could not be ratified by EPMA analyses due to the limited space resolution of this technique ($\sim 1\ \mu$m), which is much higher than the crystallite size domains observed for this phase: 35 nm. For the sake of simplicity, the segregation reaction at 550°C can be then roughly described by:

$$LaNi_5Mn_2 \xrightarrow{550^\circ C,1\ h} (79\ wt\%)\ LaNi_4Mn + (21\ wt\%)\ NiMn$$

This result is supported by the facts that the secondary phase exhibits the tetragonal AuCu-type structure, which corresponds to equiatomic NiMn [16], and that the relative mass content approaches to those obtained by Rietveld analysis (Table I). It should be noted that, on heating, Mn atoms are preferably segregated out of the over-stoichiometric structure as compared with Ni atoms. This is somehow expected as Mn is reported to preferably occupy dumbbell sites [5], which may act as nucleation centres for the segregated phase due to local depletion of La concentration.

3.2. Electrochemical properties

Key electrochemical measurements were performed for highly over-stoichiometric $LaNi_5Mn_2$ (450°C-annealing) and stoichiometric $LaNi_4Mn$ (550°C-annealing) alloys. Fig. 4 shows partial hydrogen pressures for both electrodes as obtained from equilibrium potential curves using the Nerst equation:

$$Eeq(V\ vs.\ Hg/HgO) = -0.9301 - 0.01284 LnPH_2(atm)$$

for which the activity of water in 5M KOH has been taken into account. For the over-stoichiometric $LaNi_5Mn_2$ alloy, the reversible discharge capacity reaches 135 mAh/g without exhibiting any plateau pressure. On the other hand, stoichiometric $LaNi_4Mn$ attains as much as 250 mAh/g and displays a wide plateau pressure at 0.015 atm, which resembles previous solid-gas results for this intermetallic compound [10]. For the latter alloy, only the major $LaNi_4Mn$ phase has been considered for hydrogen discharging as the NiMn phase is expected to require very high pressures for hydrogen absorption. Since Mn-content only affects hydride stability [10], differences between both electrodes as concerns their hydrogen capacity and existence of plateau pressure are unequivocally attributed to their different stoichiometric degree.

Cycle-life behaviour of both electrodes up to 55 charging/discharging cycles is shown in Fig. 5. The

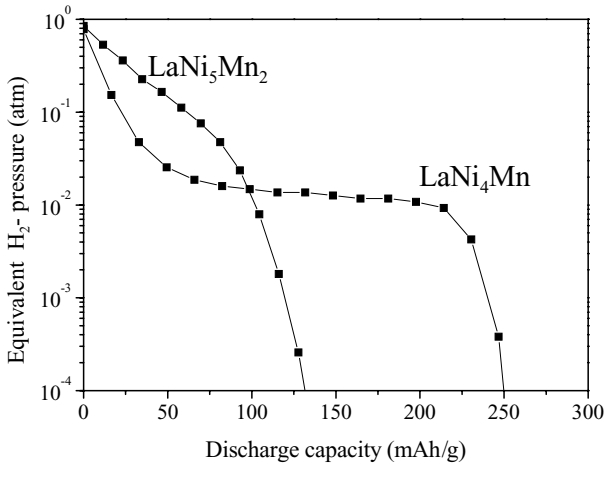

Figure 4 Electrochemical isotherms of $LaNi_5Mn_2$ and $LaNi_4Mn$ alloys.

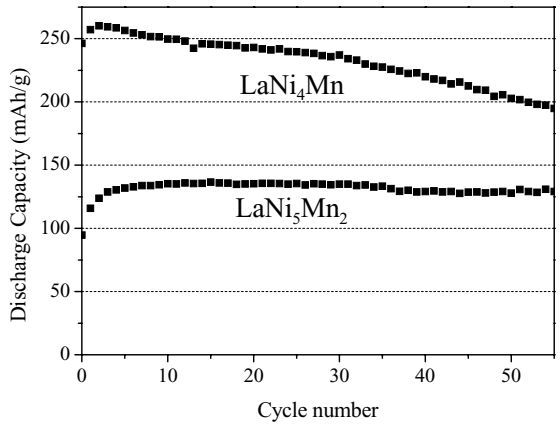

Figure 5 Reversible discharge capacity of $LaNi_5Mn_2$ and $LaNi_4Mn$ alloy electrodes as a function of the cycle number.

electrodes are completely activated after only four cycles. Maximum storage capacity is 135 mAh/g for the over-stoichiometric alloy, whereas it reaches 260 mAh/g for the stoichiometric one. As concerns capacity decay on cycling, it is only of 5% for the over-stoichiometric alloy whereas it yields 25% for the stoichiometric one. Therefore, much longer cycle-life is attained with over-stoichiometric alloys though at the cost of a reduction of the storage capacity. This result might be well related to a significant reduction of hydrogen capacity in the hydride phase on increasing stoichiometry. In this way, the wideness of the plateau pressure is strongly shortened (Fig. 4) and related internal stresses at the solute/hydride interface are reduced. This improves mechanical stability and cycle-life of the MH electrode.

4. Conclusions

By using mechanical alloying, highly over-stoichiometric $LaNi_5Mn_2$ can be obtained from biphasic $La(Ni,Mn)_5 + (Ni,Mn)$ alloy. This phase is metastable since, on heating, it decomposes back to the initial biphasic composition. Therefore, stoichiometry in $LaNi_{5+x}$-type alloys can be controlled at wish by thermal annealing of ball-milled over-stoichiometric alloys. Following this procedure, we have been able to measure key electrochemical properties of over-stoichiometric $LaNi_5Mn_2$ for being compared with those of stoichiometric $LaNi_4Mn$. Electrochemical cycle-life greatly improves with increasing stoichiometry but the electrode storage capacity diminishes. This is attributed to a reduction of internal mechanical stress in the solute/hydride alloy interface caused by a lower hydrogen capacity of the hydride phase.

Acknowledgements

The authors wish to thank E. Leroy for EPMA analyses.

References

1. J. H. N. VAN VUCHT, F. A. KUIJPERS and H. C. A. M. BRUNING, *Philips Res. Rep.* **25** (1970) 133.
2. H. OGAWA, M. IKOMA, H. KAWANO and I. MATSUMOTO, *J. Power Sources* **12** (1988) 393.
3. P. H. L. NOTTEN, R. E. F. EINERHAND and J. L. C. DAAMS, *J. Alloys Compd.* **210** (1994) 221.
4. *Idem.*, *Ibid.* **231** (1995) 604.
5. P. H. L. NOTTEN, M. LATROCHE and A. PERCHERON-GUÉGAN, *J. Electrochem. Soc.* **146** (1999) 3181.
6. K. H. J. BUSCHOW and H. H. VAN MAL, *J. Less-Common Met.* **29** (1972) 203.
7. F. CUEVAS, M. HIRSCHER, B. LUDESCHER and H. KRONMULLER, *J. Appl. Phys.* **86** (1999) 6690.
8. F. CUEVAS, M. LATROCHE, M. HIRSCHER and A. PERCHERON-GUÉGAN, *J. Alloys Compd.* **323/324** (2001) 4.
9. F. CUEVAS, J.-M. JOUBERT, M. LATROCHE, O. ISNARD and A. PERCHERON-GUÉGAN, *Appl. Phys.* A **74** (2002) S1175.
10. C. LARTIGUE, A. PERCHERON-GUÉGAN, J.-C. ACHARD and F. TASSET, *J. Less-Common Met.* **75** (1980) 23.
11. J. RODRÍGUEZ-CARVAJAL, *Physica* B **192** (1993) 55.
12. R. W. KNOLL, *Mater. Lett.* **3** (1985) 137.
13. F. CUEVAS and M. HIRSCHER, *Acta Mater.* **51** (2003) 701.
14. J. HONSTRA and K. H. J. BUSCHOW, *J. Less-Common Met.* **27** (1972) 123.
15. M. LATROCHE, J.-M. JOUBERT, A. PERCHERON-GUÉGAN and P. H. L. NOTTEN, *J. Solid State Chem.* **146** (1999) 313.
16. E. KRÉN, E. NAGY, I. NAGY, L. PAL and P. SZABO, *J. Phys. Chem. Solids* **29** (1968) 101.

Received 11 September 2003
and accepted 27 February 2004